Materials Today Bio 21 (2023) 100695

Contents lists available at ScienceDirect

Materials Today Bio

journal homepage: www.journals.elsevier.com/materials-today-bio

# Construction of 3D-Bioprinted cartilage-mimicking substitute based on photo-crosslinkable Wharton's jelly bioinks for full-thickness articular cartilage defect repair

Guanhuai Hu [a,1], Zhuo Liang [a,1], Zhenlin Fan [a,1], Mengyuan Yu [a], Qingqing Pan [a], Yan Nan [a], Wei Zhang [b,c], Lei Wang [a], Xiansong Wang [a,b,c], Yujie Hua [a,b,c,*], Guangdong Zhou [a,b,c,**], Wenjie Ren [a,***]

[a] Institutes of Health Central Plain, The Third Affiliated Hospital of Xinxiang Medical University, Clinical Medical Center of Tissue Engineering and Regeneration, Xinxiang Medical University, Xinxiang, Henan, 453003, PR China
[b] Department of Plastic and Reconstructive Surgery, Shanghai Ninth People's Hospital, Shanghai Jiao Tong University School of Medicine, Shanghai Key Laboratory of Tissue Engineering, Shanghai, 200011, PR China
[c] National Tissue Engineering Center of China, Shanghai, 200241, PR China

ARTICLE INFO

*Keywords:*
Photo-crosslinkable hydrogels
Wharton's jelly
3D bioprinting
Articular cartilage repair)

ABSTRACT

Three-dimensional (3D) bioprinted cartilage-mimicking substitutes for full-thickness articular cartilage defect repair have emerged as alternatives to *in situ* defect repair models. However, there has been very limited breakthrough in cartilage regeneration based on 3D bioprinting owing to the lack of ideal bioinks with printability, biocompatibility, bioactivity, and suitable physicochemical properties. In contrast to animal-derived natural polymers or acellular matrices, human-derived Wharton's jelly is biocompatible and hypoimmunogenic with an abundant source. Although acellular Wharton's jelly can mimic the chondrogenic microenvironment, it remains challenging to prepare both printable and biologically active bioinks from this material. Here, we firstly prepared methacryloyl-modified acellular Wharton's jelly (**AWJMA**) using a previously established photo-crosslinking strategy. Subsequently, we combined methacryloyl-modified gelatin with **AWJMA** to obtain a hybrid hydrogel that exhibited both physicochemical properties and biological activities that were suitable for 3D bioprinting. Moreover, bone marrow mesenchymal stem cell-loaded 3D-bioprinted cartilage-mimicking substitutes had superior advantages for the survival, proliferation, spreading, and chondrogenic differentiation of bone marrow mesenchymal stem cells, which enabled satisfactory repair of a model of full-thickness articular cartilage defect in the rabbit knee joint. The current study provides a novel strategy based on 3D bioprinting of cartilage-mimicking substitutes for full-thickness articular cartilage defect repair.

## 1. Introduction

Articular cartilage defect has a poor self-repair capacity owing to its avascular and aneural nature [1–3]. Usually, autologous cartilage implantation is considered the gold standard for the clinical treatment of articular cartilage defects, but there remains some shortcomings, such as limited donors, iatrogenic damage, and poor adaptation to irregular defect shapes [4,5]. Recently, tissue engineering, in which seed cells are combined with biocompatible scaffolds, has proven to be a promising alternative to current clinical treatments [6–9]. Compared with traditional polymer-based scaffolds, hydrogels can better mimic the three-dimensional (3D) microenvironment to facilitate cell proliferation, spreading, and differentiation, which enables satisfactory *in situ* articular cartilage defect repair, as previously reported [10–12].

* Corresponding author. The Third Affiliated Hospital of Xinxiang Medical University, Institutes of Health Central Plain, Clinical Medical Center of Tissue Engineering and Regeneration, Xinxiang Medical University, Xinxiang, Henan, 453003, PR China.
** Corresponding author. The Third Affiliated Hospital of Xinxiang Medical University, Institutes of Health Central Plain, Clinical Medical Center of Tissue Engineering and Regeneration, Xinxiang Medical University, Xinxiang, Henan, 453003, PR China.
*** Corresponding author.
*E-mail addresses:* yujiehua@shsmu.edu.cn (Y. Hua), guangdongzhou@126.com (G. Zhou), wjren1966@163.com (W. Ren).
[1] These authors contributed equally: Guanhuai Hu, Zhuo Liang, Zhenlin Fan.

https://doi.org/10.1016/j.mtbio.2023.100695
Received 28 March 2023; Received in revised form 30 May 2023; Accepted 6 June 2023
Available online 9 June 2023
2590-0064/© 2023 Published by Elsevier Ltd. This is an open access article under the CC BY-NC-ND license (http://creativecommons.org/licenses/by-nc-nd/4.0/).

Using the prevailing technique of 3D bioprinting, cartilage-mimicking substitutes can be individually customized with irregular morphology, large size, and biological activities for articular cartilage defect repair [13–18]. To construct the 3D bioprinted architecture, seed cells need to be encapsulated in cytocompatible and printable hydrogels to form bioinks, followed by extrusion molding to achieve the structural complexity of specific 3D shapes. Notably, bone marrow mesenchymal stem cells (BMSCs) are one of the desired seed cells for articular cartilage regeneration owing to their definite chondrogenic differentiation potential, especially in cartilage-specific microenvironments [19–21]. Thus, the key difficulty of 3D bioprinting cartilage-mimicking substitutes is the preparation of ideal bioinks that meet the following requirements: 1) favorable biocompatibility; 2) good printability; 3) suitable physicochemical properties (*e.g.*, rheological behavior and mechanical strength); 4) cartilage-specific induction activity for BMSCs. Owing to the lack of ideal bioinks that meet all these requirements, the 3D bioprinting of cartilage-mimicking substitutes remains a challenge.

Bioinks based on temperature-sensitive methacryloyl-modified gelatin (**GelMA**) and viscous hyaluronic acid (**HAMA**) are widely used because they can be easily printed, and the morphological stability of the resulting structure can be maintained through non-contact photo-crosslinking methods [22–26]. However, these universal bioinks lack tissue-specific induction activity, which impedes the reconstruction of complex extracellular matrices of multi-type tissues. Photo-crosslinkable acellular hydrogels can mimic tissue-specific extracellular matrices, such as the cartilage-, derm-, or muscle-derived acellular matrix, and undergo rapid sol-to-gel transitions upon light irradiation [27–29]. However, components of these extracellular matrices are derived from animals, and thus may cause xenografting problems in clinical translation. In contrast to the above animal-derived acellular matrices, Wharton's jelly is obtained from the human umbilical cord, which is widely available and considered a medical waste, and thus it would reduce the risk associated with xenografting [30,31]. More importantly, Wharton's jelly has emerged as a promising material for cartilage regeneration because it is similar to articular cartilage components and contains several chondrogenic growth factors, such as insulin-like growth factor-I (IGF-I) and transforming growth factor-β (TGF-β) [32]. Existing studies usually apply acellular Wharton's jelly in the form of powder additives, from which 3D specific shapes are difficult to form unless they are combined with other frameworks, such as lyophilized gelatin scaffolds or 3D-printed polymers [33,34]. Therefore, it is valuable to exploit previously established photo-crosslinking strategies to prepare both printable and biologically active bioinks based on acellular Wharton's jelly.

Herein, we developed a novel strategy for full-thickness articular cartilage defect repair using 3D-bioprinted cartilage-mimicking substitutes based on photo-crosslinkable Wharton's jelly bioinks. Methacryloyl-modified acellular Wharton's jelly (**AWJMA**) was firstly prepared through a multi-step procedure of decellularization, enzymatic digestion, methacrylatetion (MA) modification, and lyophilization. Subsequently, **GelMA** was combined with **AWJMA** to obtain hybrid photo-crosslinkable bioinks (**AWJMA/GelMA** hydrogels) with enhanced physicochemical properties and biological activities. Furthermore, BMSCs-loaded cartilage-mimicking substitutes were successfully constructed by light-assisted extrusion-based 3D bioprinting. *In vitro* experiments verified that the 3D-bioprinted cartilage-mimicking substitute was beneficial for inner BMSC survival, proliferation, spreading, and chondrogenic differentiation. Finally, a model of full-thickness articular cartilage defect in the rabbit knee joint was treated with the BMSCs-loaded 3D-bioprinted cartilage-mimicking substitute, revealing satisfactory repair of the articular cartilage defect.

## 2. Materials and methods

### 2.1. Materials

In this study, trypsin, pepsin, acetic acid, dexamethasone, methacrylic anhydride, sodium hydroxide, and lithium phenyl-2,4,6-trimethylbenzoylphosphinate (LAP) were purchased from Sigma-Aldrich. ITS were purchased from ScienCell. TGF-β1 were purchased from R&D Systems Inc. All other chemicals were reagent grade, and deionized water was used.

### 2.2. Preparation of acellular Wharton's jelly (AWJ)

**AWJ** was prepared with reference to a previous method [35] using umbilical cords, which were collected after obtaining informed consent of donors. All tissue samples were rinsed with phosphate-buffered saline (PBS) containing 2% penicillin/streptomycin solution to remove residual blood. After carefully taking off blood vessels and redundant connective tissues from the umbilical cords, Wharton's jelly was minced into small fragments. Then, the fragments were decellularized with 1 M NaOH solution for 3 h at room temperature, generating **AWJ**. Thereafter, **AWJ** was homogenized into a suspension slurry using a tissue disintegrator, followed by digestion with pepsin supplemented with acetic acid (pH = 2–3) at 37 °C for 24 h. After neutralization to pH = 7.4 by using NaOH, the slurry was then centrifuged (5000 rpm, 5 min), and the supernatant was lyophilized to obtain **AWJ**.

### 2.3. Synthesis of AWJMA and GelMA

The **AWJ** solution was prepared by dissolving 0.5 g of **AWJ** in 200 mL of deionized water with stirring, and 0.5 mL methacrylic anhydride was added at a rate of 0.5 mL/min in an ice bath. The pH was maintained between 8 and 10 with 5 M NaOH, and the reaction continued overnight under constant stirring. After the reaction completed, the solution was centrifuged to remove insoluble substances, and the pH was adjusted to 7.4 with 0.5 M HCl. Then, the product was dialyzed using a 3500 Da dialysis membrane in distilled water for 1 week, followed by freezing and lyophilizing.

Methacryloyl modification of gelatin was performed as previously reported [36]. Briefly, A total of 10 g of gelatin was dissolved in 200 mL of PBS (pH = 7.4) and stirred vigorously at a constant speed using a magnetic stirrer at 50 °C. Methacrylate anhydride (8 mL) was slowly added and allowed to react with gelatin for 3 h. The solution was collected, and the portion that did not react was removed under 5000 rpm centrifugation. Then, the solution was dialyzed at 40 °C for 1 week using a dialysis membrane (7000 Da). The dialyzed reaction solution was lyophilized to acquire **GelMA**.

### 2.4. Proteomic analysis of acellular Wharton's jelly

To prepare the samples for proteomic analysis, **WJ** and **AWJ** powders were dissolved and cracked to extract proteins. After measuring the protein levels, each protein sample was digested with trypsin overnight at 37 °C, and the peptides were desalted and quantified. Trypsin-digested peptides were analyzed using liquid chromatography (LC) with tandem mass spectrometry (MS/MS) performed on an EASY-nLC 1200 nanoflow system (Thermo, USA) connected to a Q Exactive HF-X quadrupole Orbitrap mass spectrometer (Thermo, USA) equipped with a nano-electrospray ion source. MS/MS spectra were searched using Proteome-DiscovererTM Software 2.4. The false discovery rate (FDR) of peptide identification was set to FDR ≤0.01. A minimum of one unique peptide identification was used to support protein identification. Annotation of all identified proteins was performed using GO (http://geneontology.org/) and KEGG pathways (http://www.genome.jp/kegg/). Differential expressed proteins (DEPs) were further used for GO and KEGG enrichment analyses.

### 2.5. Characterization of AWJMA and GelMA

**AWJMA** and **GelMA** were analyzed using Fourier-transform infrared (FTIR) spectroscopy (Thermo Nicolet Nexus 470, USA), and methacryloyl

modification of **AWJ** and gelation was confirmed using $^1$H nuclear magnetic resonance (NMR) spectroscopy (Bruker 700 MHz Advance, Switzerland) and $D_2O$ as the solvent.

### 2.6. Hydrogel preparation

Unless otherwise stated, all concentrations are given as a percentage of weight per volume (w/v). **GelMA** (800 mg, 8 wt%), **AWJMA** (200 mg, 2 wt%), and lithium acylphosphinate (LAP) (0.25 wt%) were dissolved in 10 mL of PBS solution (pH 7.4) to obtain the **AWJMA/GelMA** hydrogel. The **GelMA** hydrogel consisted of **GelMA** (10 wt%) and LAP (0.25 wt%) in 10 mL of PBS solution (pH 7.4). The **AWJMA** hydrogel consisted of **AWJMA** (10 wt%) and LAP (0.25 wt%) in 10 mL of PBS solution (pH 7.4). All hydrogel formulations were fully mixed with continuous stirring, sterilized with syringe filters (0.22 μm pore size). Finally, the hydrogel formulations were photo-crosslinked by exposure to blue light at the wavelength of 405 nm using a light-emitting diode (LED) source (Uvata Precision Optoelectronics Co., Ltd.) with an intensity of 20 mW/cm$^2$ for an exposure time of 30 s.

### 2.7. Morphology observation

The microstructure of lyophilized **AWJMA/GelMA** hydrogel, **AWJMA** hydrogel, and **GelMA** hydrogel samples were observed using scanning electron microscopy (SEM) at an accelerating voltage of 3 keV (ZEISS Gemini 300). All samples were sputtered with gold for 45 s (Oxford Quorum SC7620) before observation.

### 2.8. Rheological analysis

Dynamic rheology experiments were performed on a HAAKE MARS III photorheometer using a parallel plate with a diameter of 20 mm (P20 TiL) and an ultraviolet light curing system (OmniCure Series 2000) operated at 20 mW/cm$^2$. Time sweep oscillatory tests were performed at 10% strain (CD mode) with a frequency of 1 Hz and gap of 0.5 mm for 70 s. Temperature-sweep oscillatory tests were performed at 10% strain (CD mode) and 1 Hz frequency parameters from 60 to 0 °C. The sol-to-gel transition point was determined as the time when the storage modulus (G″) surpassed the loss modulus (G″).

### 2.9. Testing of mechanical properties

Mechanical tests of as-prepared hydrogels were carried out using a INSTRON 5542 universal material testing machine with a capacity of 500 N. For compression tests at the speed of 1 mm/min, hydrogel samples were prepared as cylinders with a diameter of 5 mm and length of 4 mm. The hydrogels were subjected to compression tests after complete gelation under light irradiation using a 405-nm LED at a power of 20 mW/cm$^2$.

### 2.10. Equilibrium porosity and swelling ratio

The porosity (average void volume) of the hydrogels was determined using alcohol. All experiments were performed in triplicate. Freeze-dried hydrogels were immersed in a sealed tube containing alcohol for 24 h, at which the weight of the sample ($W_{24}$) was constant. The actual volume (Va) of the sample was calculated using the following formula:

$$\mathrm{Va} = (W_{24} - W_0) / p,$$

where $W_{24}$, and $W_0$ are respectively the weight of the sample at 24 h and 0 h, and $p$ is the density of alcohol (0.785 g/cm$^3$). The porosity was determined using the following equation:

$$\text{Porosity } (\%) = \mathrm{Va}/\mathrm{Ve} \times 100\%,$$

where Ve is the exterior volume of each sample.

The swelling behavior of the **AWJMA/GelMA** hydrogel, **AWJMA** hydrogel and **GelMA** hydrogel was investigated using the gravimetric method. Briefly, lyophilized or wet **AWJMA/GelMA** hydrogel, **AWJMA** hydrogel, and **GelMA** hydrogel samples were immersed in PBS at 37 °C and weighed after 2, 4, 6, 12, 24, and 36 h. Excess water on the surface of the sample was absorbed with filter paper. The wet weight of each sample (Ws) was measured with an electronic balance. The swelling ratio was calculated using the following equation:

$$\text{Swelling ratio } (\%) = (W_s - W_d)/W_d \times 100\%,$$

where Ws is the swollen weight of the hydrogel sample in the swelling state at equilibrium and $W_d$ is the dry weight of the lyophilized hydrogel sample.

### 2.11. In vitro collagenase degradation

The dry weight of the **AWJMA/GelMA** hydrogel, **AWJMA** hydrogel, and **GelMA** hydrogel were recorded as $W_0$. Then, the gel was incubated in Dulbecco's PBS (D-PBS) (pH = 7.4) supplemented with collagenase solution (1 U/mL in D-PBS). At each time point, these samples were collected and washed with distilled water. The washed samples were lyophilized using a freeze-drying machine. Then, the weight of each lyophilized sample ($W_t$) was measured using an electronic balance. The mass loss (%) was calculated according to the following equation:

$$\text{Degradation ratio } (\%) = (W_0 - W_t)/W_0 \times 100\%,$$

where $W_0$ is the dry weight of the hydrogel sample without D-PBS incubation and $W_t$ is the dry weight of this hydrogel sample following D-PBS incubation with the time indicated.

### 2.12. Cytocompatibility evaluation

BMSCs were obtained from the bone marrow of adult rabbits, and harvested, cultured, and expanded in the culture medium at 37 °C with 5% $CO_2$ of incubator, medium was changed every two days to ensure sufficient nutrient supply to the cells. Cells were used when they expanded into the second generation.

The cytocompatibility of the **AWJMA/GelMA** hydrogel was evaluated using the live/dead staining assay and cell counting kit-8. For live/dead staining, $3 \times 10^5$ cells were mixed in 100 μL of the pregel solution of the **AWJMA/GelMA** hydrogel before gelation. After the cells were cultured in the medium for 1, 4, 7, and 14 days, the **AWJMA/GelMA** hydrogel was stained with 2 μg/mL fluorescein in diacetate at 37 °C for 15 min and 5 μg/mL propidium iodide at 37 °C for 5 min. The cells were evaluated under a fluorescence microscope. For the cytotoxicity assay, BMSCs were seeded in 96-well plates at a concentration of 1000 cells per well and cultured for 24 h. The medium was replaced with a series of fresh medium containing **AWJMA** powder (0, 0.025%, 0.05%, 0.1%, 0.2%, or 0.4% w/v). The culture solution was removed after 1, 4, and 7 days of incubation, and 10 μL of CCK-8 reagent and 100 μL of culture medium were added to each well, and the cells were incubated for 2 h at 37 °C. The absorbance at 450 nm was measured using a microplate reader (Synergy H1, BioTek).

### 2.13. In vitro chondrogenic induction experiments

*In vitro* chondrogenic capacity was determined by RT-qPCR and immunofluorescence staining. For RT-qPCR, BMSCs were seeded in 6-well plates at a concentration of $2 \times 10^5$ cells per well and cultured for 24 h. The medium was then replaced with cartilage induction medium, which was supplemented with 0.4% **AWJ** powder for one group. In addition, BMSCs were cultured in common low-sugar DMEM medium, set as the Control group. Then, the expression levels of cartilage-related

genes, such as *COL2*, aggrecan (*ACAN*), and *SOX9*, of all groups were evaluated.

For immunofluorescence staining, BMSCs-loaded **GelMA** and **AWJMA/GelMA** hydrogels were prepared as cylinders (6 mm diameter, 2 mm height), and 6 mL of pre-warmed chondrogenic culture medium (High-sugar DMEM medium with 10 ng/mL of TGF-β1, 40 ng/mL of dexamethasone, 1.25 mg/mL of bovine serum albumin, 1% ITS, and 1% antibiotic-antimycotic) was carefully overlaid on each gel and changed every three days during *in vitro* culturing. After 28 days, COL2 immunofluorescence staining was used to determine cartilaginous induction.

### 2.14. 3D printing of AWJMA/GelMA hydrogel scaffolds

Before printing, pregel solutions of **AWJMA/GelMA** hydrogel with LAP (0.25 w/v%) in PBS buffer were prepared. Porous hydrogel scaffolds were fabricated using a three-axis positioning system (3D Bio-Architects working station, Regenovo, China). For cell-free printing, gel precursors were directly used or dyed with Safranin-O. The gel precursor was loaded separately into 5-mL syringes and then extruded through a nozzle with an inner diameter of 0.21 mm to deposit a physical gel at 18 °C, followed by exposure to LED light (405 nm, 20 mW/cm$^2$) for 1 min. During the printing process, relevant printing parameters, such as applied pressure, printing speed, and interfilament gap, were tested separately. For bioprinting, BMSCs were mixed homogeneously in the bioink at the last step. Immediately after bioprinting, the bioprinted constructs were incubated in DMEM supplemented with 10% fetal bovine serum (FBS) and 1% penicillin/streptomycin at 37 °C under 5% $CO_2$. Each step was strictly conducted under sterile conditions. To demonstrate the biological functions of bioprinted tissues, live/dead staining and phalloidin-FITC/DAPI staining were performed at 1, 4, and 7 days. Live/dead staining was performed as described in Section 2.13. For phalloidin-FITC/DAPI staining, at designated time points of culturing, the bioprinted tissues were first fixed with 4% paraformaldehyde for 30 min and then treated with 0.1% w/v Triton X-100 in PBS for 15 min to permeabilize the cell membrane. After PBS leaching and washing, 5 μg/mL Gobbi cyclic peptide solution was added dropwise, and the cells were incubated for 1 h. After washing with PBS, the specimen was incubated in DAPI solution at 1:1000 dilution for 5 min in darkness, and the nucleus was stained. Finally, the samples were examined using confocal laser scanning microscopy (CLSM) (Leica, TCS SP8 STED3X).

### 2.15. Repair of rabbit articular cartilage defect

New Zealand white rabbits weighing 2.5–3.0 kg were used in accordance with protocols approved by the Animal Research Committee of Xinxiang Medical University (XYLL-20210288). After general anesthesia, rabbit knee joints were opened using a medial parapatellar approach. A full-thickness cylindrical defect (4 mm in diameter, 3 mm in depth) was created on the patellar groove of the femur in both legs using a sterile drill. The articular cartilage defects of rabbit models were randomly classified into three groups: (A) untreated group; (B) scaffold alone group; and (C) BMSCs-loaded scaffold group.

### 2.16. Gross morphology evaluation, histological examination, and evaluation after 6 and 12 weeks

Specimens were harvested 6 and 12 weeks after the operation, and macroscopic evaluations were conducted by three blinded observers. The International Cartilage Repair Society (ICRS) gross scoring system was used to assign scores for the degree of repair, integration, surface regularity, and total judgment. All samples were fixed in 4% paraformaldehyde, decalcified in 12% (w/v) ethylenediamine-tetra acetic acid (EDTA), dehydrated through an ethanol series, embedded in paraffin, and sectioned for histological analysis. Hematoxylin and eosin (H&E) staining, Safranin-O staining, and COL2 immunohistochemical staining of sections were used to evaluate histological structures and cartilage specific ECM deposition in repaired regions. The osteochondral joints at 6 and 12 weeks were evaluated using a histological grading system, namely the modified O'Driscoll histology scoring system (MODS).

### 2.17. Statistical analysis

All data are expressed as mean ± standard deviation with at least $n = 3$. Unpaired Student's *t*-tests were used to evaluate the differences between the groups, and values of $^*p < 0.05$, $^{**}p < 0.01$, $^{***}p < 0.001$ and $^{****}p < 0.0001$ were considered statistically significant (see Fig. 1).

## 3. Results

### 3.1. Preparation and characterization of methacrylate-modified Wharton's jelly

In this study, Wharton's jelly (**WJ**) was used to prepare methacryloyl-modified acellular Wharton's jelly (**AWJMA**) through a multi-step procedure of decellularization, enzymatic treatment, MA modification, and lyophilization. As shown in Fig. 2A and **S1**, by removing the outer membranes and blood vessels of the umbilical cords, followed by decellularization, bulk **AWJ** samples were slightly transparent. After enzymatic digestion (1 mg/mL pepsin in acetic acid solution, pH = 2–3) and lyophilization, water-soluble **AWJ** products were obtained. Then, MA modification of **AWJ** was adopted to prepare **AWJMA**. Methacrylic anhydride was mixed with the **AWJ** solution under suitable conditions, followed by dialysis and lyophilization. To characterize the MA graft of the **AWJMA** polymer, $^1$H NMR and FTIR spectra were collected. As shown in Fig. 2B and **S2**, the characteristic peaks of methacrylamide at 5.4 and 5.6 ppm appeared after the MA modification of the **AWJ** polymer, indicating successful synthesis of the **AWJMA** polymer. The typical absorption peak of C═C stretching vibration at 1452 cm$^{-1}$ region was observed in the FTIR spectrum of the **AWJMA** polymer, which was absent from the spectrum of **AWJ** polymer, further confirming the successful addition of C═C bonds (Fig. 2C).

Acellular Wharton's jelly is considered a cartilage-mimicking biomaterial that can emulate the intricacy of the native microenvironment. First, histological results showed that there were less cellular components in the **AWJ** sample than in native tissue, confirming the maximal clearance of cellular and genetic components of the ECM (Fig. 2D). Furthermore, to identify the ECM components retained after the decellularization treatment, both **WJ** and **AWJ** samples were processed for proteomics analysis. As shown in Fig. 2E and 339 unique proteins were found in the native tissue, whereas 307 unique proteins were found in decellularized Wharton's jelly. The scatter diagram and hierarchical clusters further revealed that the proteome of acellular Wharton's jelly was not significantly different from that of the native tissue (Fig. 2F and G). Furthermore, GO and KEGG pathway results indicated that the differential proteins were mainly enriched in focal adhesion and ECM-receptor interaction pathways (Fig. 2H and I), which confirmed that **AWJ** reserved most of the ECM components. Notably, TGF-β and IGF growth factors were found in both **WJ** and **AWJ** samples, which may play important roles in chondrogenic differentiation, a process that relies on the TGF-β pathway.

### 3.2. Physicochemical properties of AWJMA/GelMA hydrogels

To obtain an ideal hydrogel formulation with both mechanical strength and biological activity, **GelMA** polymer was added to bioactive **AWJMA** polymer to prepare **AWJMA/GelMA** hydrogels. As shown in Fig. 3A, light irradiation (405 nm, 20 mW/cm$^2$) induced the sol-to-gel transition to produce **AWJMA/GelMA** hydrogels, as well as **GelMA** and **AWJMA** hydrogels. To further evaluate the physicochemical properties of **AWJMA/GelMA** hydrogels, $^1$H NMR spectra, rheological and compressive experiments were performed. The $^1$H NMR spectra revealed

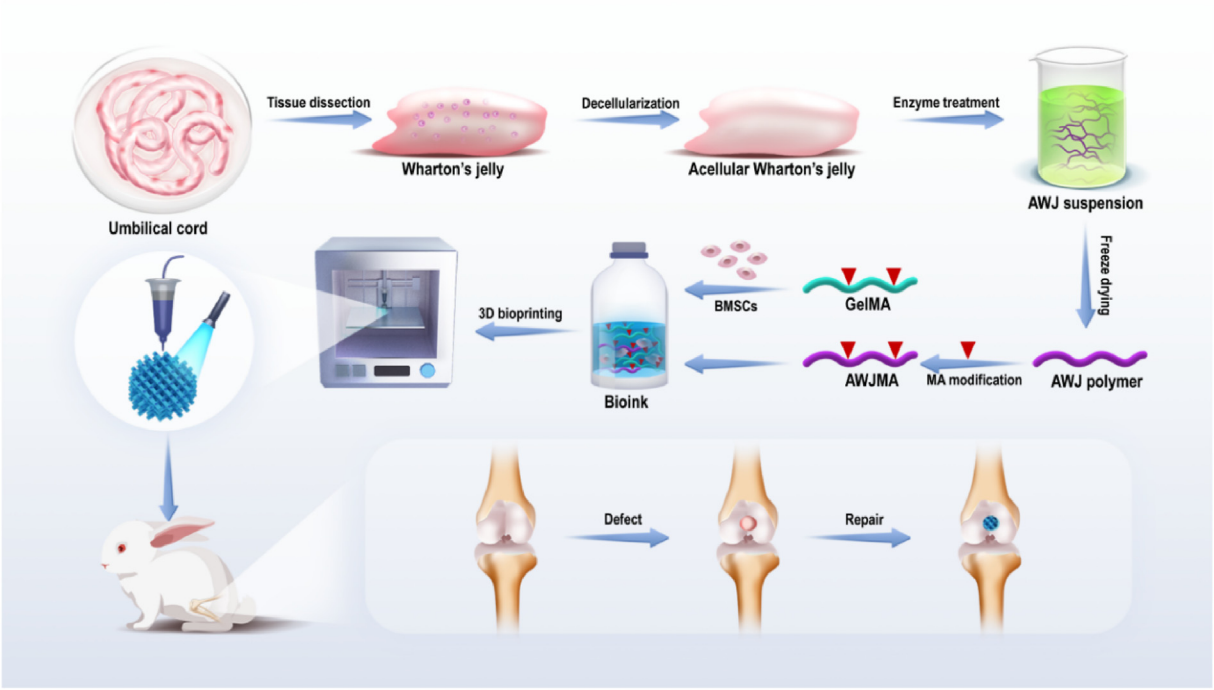


**Fig. 1.** Schematic illustration of 3D-bioprinted cartilage-mimicking substitute based on photo-crosslinkable Wharton's jelly bioinks for full-thickness articular cartilage defect repair.

that the methacrylate peak at 5.4 and 5.6 ppm distinctly decreased in intensity, indicating successful polymerization of the methacrylate groups (Fig. 3B). As shown in Fig. 3C and D, time-dependent sweep tests showed that **AWJMA** hydrogels (gel point = 9.4 ± 1.1 s) underwent relatively slow gelation, whereas both **GelMA** (gel point = 4.1 ± 0.7 s) and **AWJMA/GelMA** hydrogels (gel point = 5.0 ± 0.6 s) underwent fast gelation. Additionally, the shear modulus of the single-component **AWJMA** gel (133.7 ± 5.7 Pa) was significantly increased by introducing the **GelMA** polymer (6240 ± 400 Pa), which produced the **AWJMA/GelMA** gel with an intermediate modulus (4608 ± 125.5 Pa) owing to the dual-crosslinked network (Fig. 3E). As shown in Fig. 3F–H, the **AWJMA** gel was rigid (Young's modulus = 0.27 ± 0.02 MPa) but brittle (maximum stress = 0.07 ± 0.008 MPa), whereas the **GelMA** gel was soft (Young's modulus = 0.11 ± 0.01 MPa) and ductile (maximum stress = 0.36 ± 0.03 MPa). By combining **AWJMA** and **GelMA** components, the resulting compressive properties were satisfactory for the following experiments (Young's modulus = 0.11 ± 0.01 Pa; maximum stress = 0.29 ± 0.04 MPa).

Furthermore, SEM images showed that **GelMA**, **AWJMA**, and **AWJMA/GelMA** hydrogels had a highly porous and interconnected structure (Fig. 4A), which facilitates the exchange of nutrients and wastes. It should be noted that the pores of lyophilized **AWJMA** hydrogel were smaller than those of the other two groups (Fig. 4B), suggesting that the **AWJMA** hydrogel differed from the other two hydrogels in both composition and crosslinking density. In addition, the degradation of the **AWJMA** hydrogel in a collagenase solution was slower than those of the other two hydrogels under the same conditions (Fig. 4C). Moreover, the swelling ratio of the **AWJMA** hydrogel was larger than those of the **GelMA** and **AWJMA/GelMA** hydrogels (Fig. 4D and **S3**), indicating that the **AWJMA** hydrogel contained a higher amount of hydrophilic groups than the other two hydrogels. This also suggested that the **AWJMA** hydrogel contained more complex components than the **GelMA** hydrogel.

All these results demonstrate that the **AWJMA/GelMA** hydrogel is a promising tissue-engineered scaffold because it has suitable rheological and mechanical properties as well as a reasonable swelling ratio and degradation rate.

### 3.3. Biological properties of AWJMA/GelMA hydrogels

The biocompatibility of hydrogels is critical for cartilage regeneration. Thus, the biocompatibility of the **AWJMA/GelMA** hydrogel was first assessed using the CCK-8 assay and live/dead staining. Following coincubation with different concentrations (0, 0.025, 0.05, 0.1, 0.2, and 0.4% wt) of **AWJMA** polymers for 1, 4, and 7 days in DMEM culture medium, BMSCs showed good proliferation. Notably, cell viability in the group of 0.4% **AWJMA** polymers was significantly higher than those of the other groups on day 7 (Fig. 5A and **S4**), indicating that acellular Wharton's jelly is conductive to cell proliferation. Live/dead fluorescence staining demonstrated that BMSCs grew well and spread in the **AWJMA/GelMA** hydrogel after 4 days of culturing owing to the existence of the adhesive protein in the hybrid hydrogel formulation (Fig. 5B). After the addition of the **AWJ** polymer (0.4 wt%) to the chondrogenic culture medium (CCM) solution, the expression of cartilage-specific genes (*ACAN*, *COL2*, and *SOX9*) was significantly upregulated (Fig. 5C). Furthermore, the results of immunofluorescence staining (Fig. 5D) indicated that the BMSCs-loaded **AWJMA/GelMA** hydrogel expressed a greater amount of COL2 than the **GelMA** hydrogel after co-culturing in CCM for approximately 28 days, consistent with the proteomic results (Fig. 2G–I). All these results demonstrate that **AWJMA/GelMA** hydrogels not only have good biocompatibility but also promote the growth, spreading, and chondrogenic differentiation of cells.

### 3.4. 3D bioprinting of BMSCs-loaded AWJMA/GelMA hydrogels

Next, we investigated the printability of our designed **AWJMA/GelMA** hydrogels as bioinks, which usually relies on inherent physical properties, such as viscosity and temperature sensitivity. As shown in Fig. 6A, the **AWJMA** gel precursor was in a dilute solution state without any temperature-sensitive property. However, the **GelMA** component induced both **GelMA** and **AWJMA/GelMA** gel precursors to undergo temperature-sensitive sol-to-gel transitions, which is essential for extrusion-based 3D bioprinting. Therefore, the **AWJMA/GelMA** gel precursor was inherently printable and first loaded into the printing syringe at a low temperature (18 °C) to form a physical gel that could be

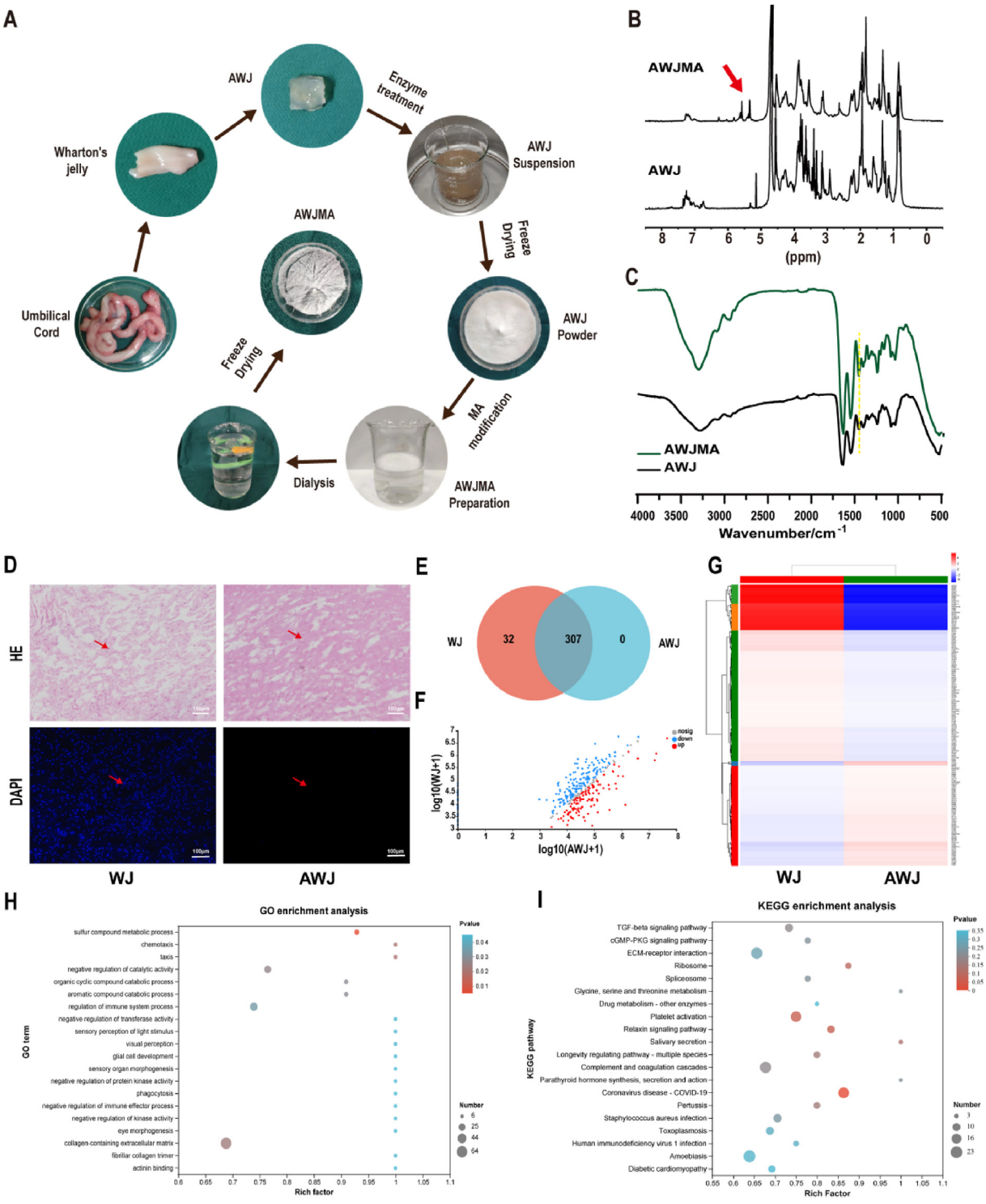


**Fig. 2. Preparation and characterization of methacryloyl-modified Wharton's jelly.** A) Synthesis of **AWJMA** polymer through decellularization, enzymatic treatment, MA modification, and lyophilization treatment. B, C) $^{1}$H NMR (B) and FTIR (C) spectra of **AWJMA** and **AWJ** polymers. D) Histological images of H&E and DAPI staining of Wharton's jelly before and after decellularization. E) Venn diagram showing the number of proteins identified in Wharton's jelly and AWJ powder. F) Scatter diagram showing the significantly high-retention (red dots, FC > 2, *P* value < 0.05) and low-retention (blue dots, FC < 0.5, *P* value < 0.05) proteins in **AWJ** versus Wharton's jelly. G) Heatmap and hierarchical cluster analysis using protein expression data from **AWJ** and Wharton's jelly. E) GO enrichment analysis and H) KEGG enrichment analysis of differentially reserved proteins in **AWJ** and Wharton's jelly, showing the top 20 enrichment terms.

extruded without collapsing. Then, the 3D printed constructs were further stabilized by photo-crosslinking with blue-light irradiation (Fig. 6B). Moreover, the main printing parameters, namely applied pressure, printing speed, and interfilament gap, were investigated to obtain the optimum printing resolution with the **AWJMA/GelMA** hydrogel. As shown in Fig. 6C, for a printing needle with a diameter of 210 μm, the applied pressure was optimized to 0.35 MPa (printing diameter = 271 ± 39 μm), and the printing speed was optimized to 10 mm/s (printing diameter = 254 ± 28 μm). Additionally, a series of hydrogel scaffolds with different interfilament gaps was printed (the

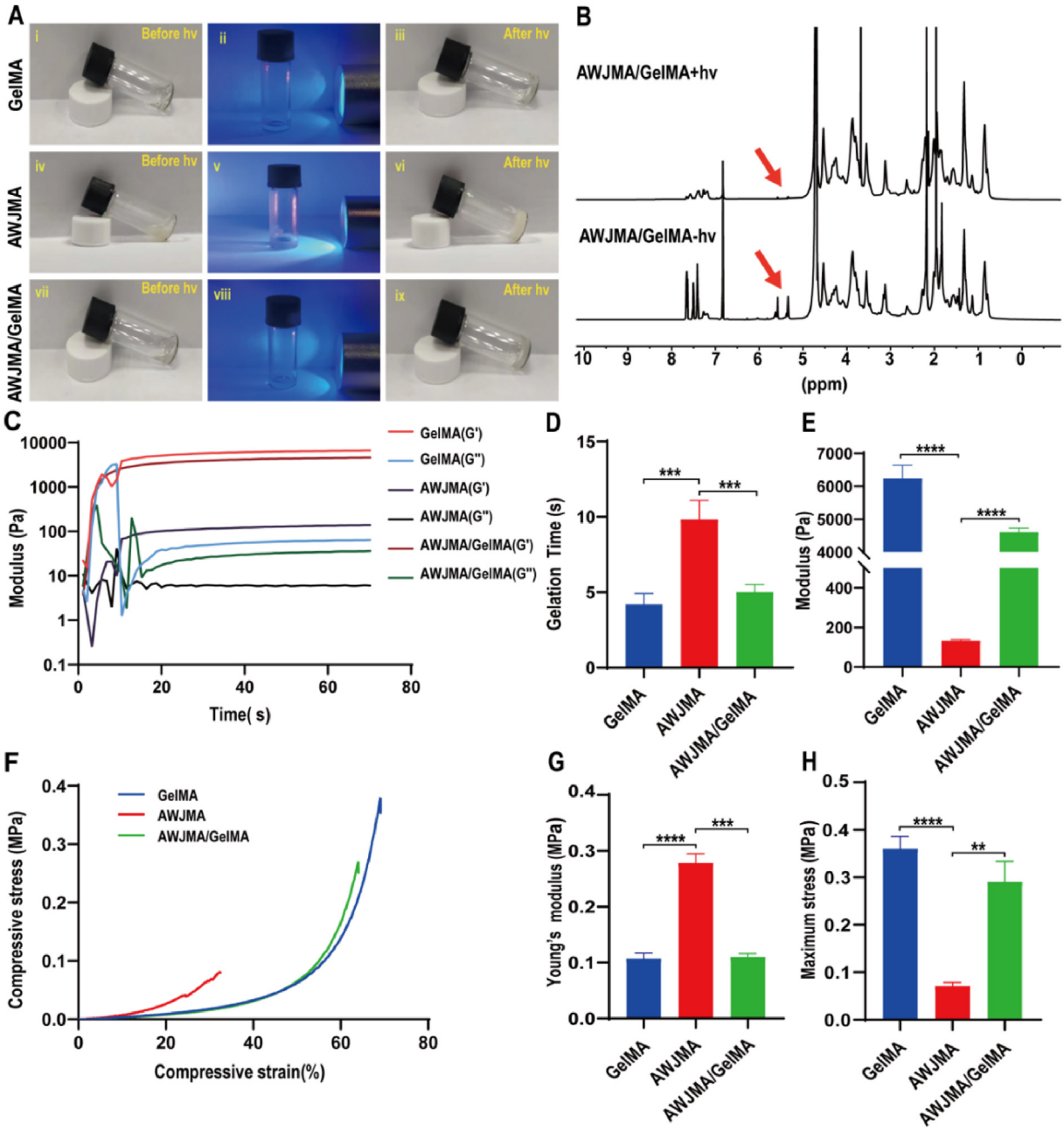


**Fig. 3. Physicochemical properties of GelMA, AWJMA, and AWJMA/GelMA hydrogels.** A) Photographs showing the sol-to-gel transitions of **GelMA**, **AWJMA**, **AWJMA/GelMA** upon light irradiation (405 nm, 20 mW/cm$^2$). B) $^1$H NMR spectra confirming the photoinitiated polymerization of the **AWJMA/GelMA** hydrogel. Red arrows represent methacrylate peaks of the **AWJMA/GelMA** mixture. C) Time-sweep rheological analyses of photo-crosslinkable hydrogels with different components. D, E) The gelation time (D) and storage moduli (E) of **GelMA**, **AWJMA**, **AWJMA/GelMA** hydrogels. F–H) The compression analysis (F), Young's modulus (G), and maximum stress (H) of **GelMA**, **AWJMA**, and **AWJMA/GelMA** hydrogels. $^{**}p < 0.01$, $^{***}p < 0.001$, $^{****}p < 0.0001$.

center distance of the printing filaments was preset to 1.0, 1.5, or 2.0 mm), and satisfactory morphological fidelity was achieved with the interfilament gap of 1.5 mm under 0.35 MPa printing pressure and 10 mm/s printing speed (Fig. 6D and E). To investigate the cytocompatibility of 3D-bioprinted lattice constructs, BMSCs-loaded **AWJMA/GelMA** hydrogels were used for printing in the following experiments. The results of live/dead staining and phalloidin-FITC/DAPI staining revealed that BMSCs exhibited good cell viability, spreading, and proliferation in the 3D-bioprinted **AWJMA/GelMA** hydrogel after 7 days of culturing *in vitro* (Fig. 6F and **S5**). Overall, 3D-bioprinted **AWJMA/GelMA** hydrogel scaffolds have suitable 3D-printing characteristics and ideal cytocompatibility for BMSC cultures *in vitro*.

### 3.5. Repair of full-thickness articular cartilage defect in rabbit

To investigate the repair efficacy of 3D-bioprinted cartilage-mimicking substitutes, models of cylindrical full-thickness cartilage defects (4 mm in diameter and 3 mm in depth) in rabbits were created. The defects were repaired with BMSCs-loaded 3D-bioprinted **AWJMA/GelMA** hydrogels as the experimental group and BMSCs-free 3D-bioprinted **AWJMA/GelMA** hydrogels as the control group (Fig. 7A). The rabbits were sacrificed and collected for gross observation (Fig. 7B) and histological examinations at 6 and 12 weeks post-surgery. In the untreated group at 6 weeks and 12 weeks post-surgery, the gross view showed that obvious defects were repaired with fibrous-like tissue in the cartilage layer. In the control group, the defects were distinctly repaired

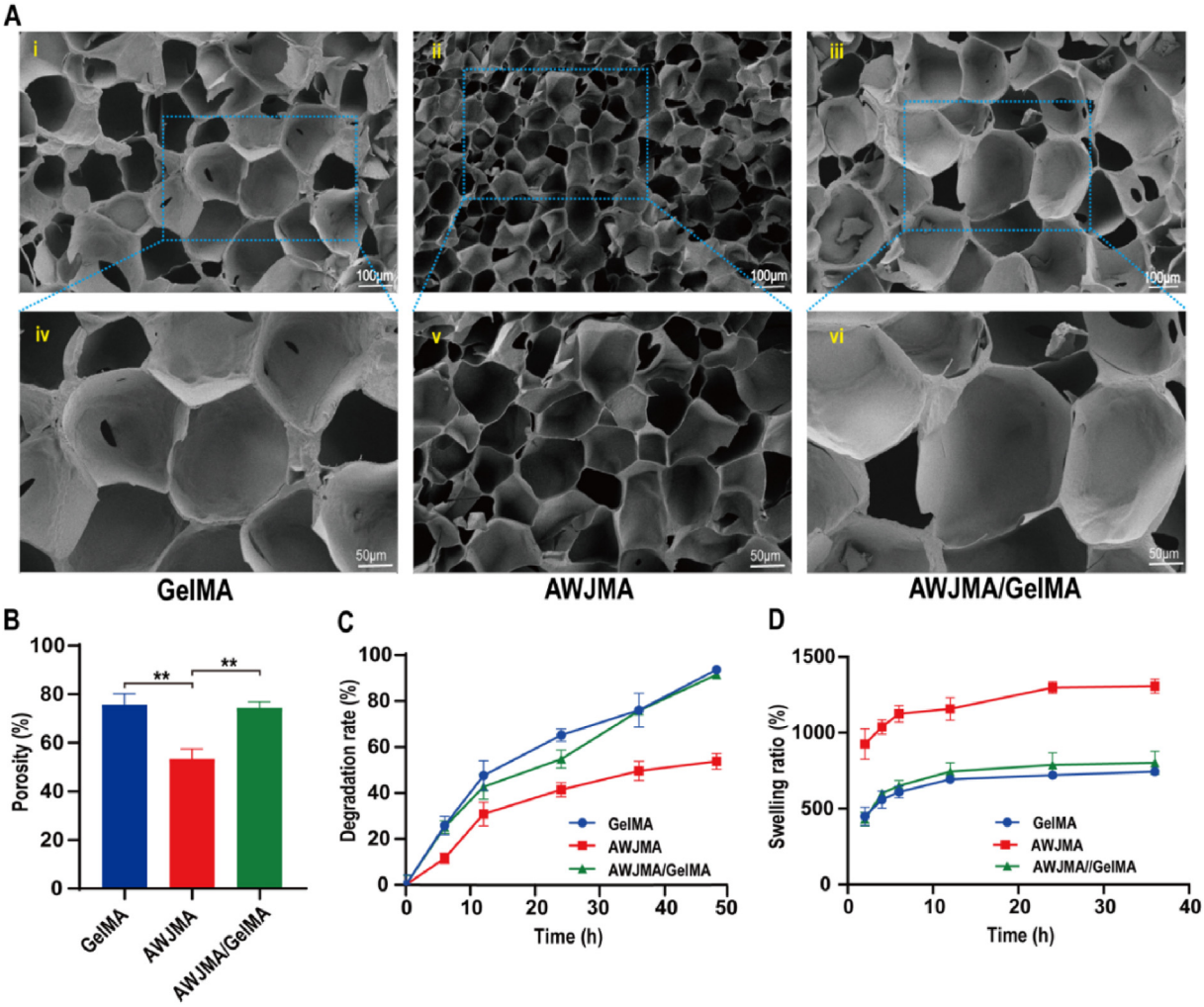


**Fig. 4. Characterization of hydrogel structure, swelling ratio, and degradation rate.** A) SEM images of lyophilized **GelMA**, **AWJMA**, and **AWJMA/GelMA** hydrogels. B) Open porosity of lyophilized hydrogels with different components. C) The degradation rate of **GelMA**, **AWJMA**, and **AWJMA/GelMA** hydrogels in collagenase solutions (1 U/mL). D) The swelling rate of **GelMA**, **AWJMA**, and **AWJMA/GelMA** hydrogels at dried condition. $*p < 0.05$, $**p < 0.01$, $***p < 0.001$.

with fibrous/cartilaginous hybrid tissue at 6 weeks, which gradually grew into immature cartilage tissues with unsatisfactory interfacial integration at 12 weeks post-surgery. In the experimental group, the regenerated cartilage tissue was mature and the interfacial integration was seamless without an obvious boundary at 6 and 12 weeks post-surgery.

Histological examinations of H&E staining, Safranin-O staining, and type II collagen immunofluorescence staining further confirmed the above observations (Fig. 7C and 8A). The untreated group was mainly repaired by fibrous tissue at both 6 and 12 weeks and showed visible hierarchical chaotic tissue at the edge of the defects. Notably, the untreated group presented obvious structural collapse from the injured calcified layer sustained during the creation of the full-thickness cartilage defect. In the control group, the cartilage region was also repaired by fibrous/cartilaginous hybrid tissue at 6 weeks, and the subchondral bone region was relatively better than that of the untreated group. At 12 weeks post-surgery, the cartilage area showed immature cartilage tissue filling and some clusters of the regenerated tissue. Consistent with the gross observation, the cartilage region in the experimental group was mainly repaired by the regenerated cartilaginous tissue with a relatively smooth cartilage surface, normal hyaline cartilage thickness, and seamless interfacial integration between the neocartilage and surrounding native cartilage as well as specific ECM staining with positive Safranin-O and COL2 staining at 6 weeks post-surgery. Notably, the quality of cartilage regeneration in the 6-week experimental group was better than that in the 12-week control group, indicating that BMSCs introduced to the local tissue had an important role in cartilage regeneration. At 12 weeks post-surgery, the regenerated cartilage in the experimental group was similar to the native cartilage, with a clear interface between the bone and cartilage as well as satisfactory interface integration with normal cartilage tissue. Furthermore, ICRS macroscopic scores and MODS histological scores were used to quantify the macroscopic and histological cartilage repair findings of the specimens. As shown in Fig. 8B and C, ICRS and MODS scores of the experimental group were higher than those of the other two groups, indicating that articular cartilage defect repair was more effective with the BMSCs-loaded 3D-bioprinted cartilage-mimicking substitute than with the other treatments.

## 4. Discussion

In the current study, we developed a novel strategy for the construction of 3D-bioprinted cartilage-mimicking substitutes for full-thickness articular cartilage defect repair. First, **AWJMA** was successfully prepared through a multi-step procedure of decellularization, enzymatic digestion, MA modification, and lyophilization, and the potential of **AWJMA** to support chondrogenic differentiation was confirmed. Then, we showed that hybrid **AWJMA/GelMA** hydrogels had suitable rheological and mechanical properties as well as reasonable

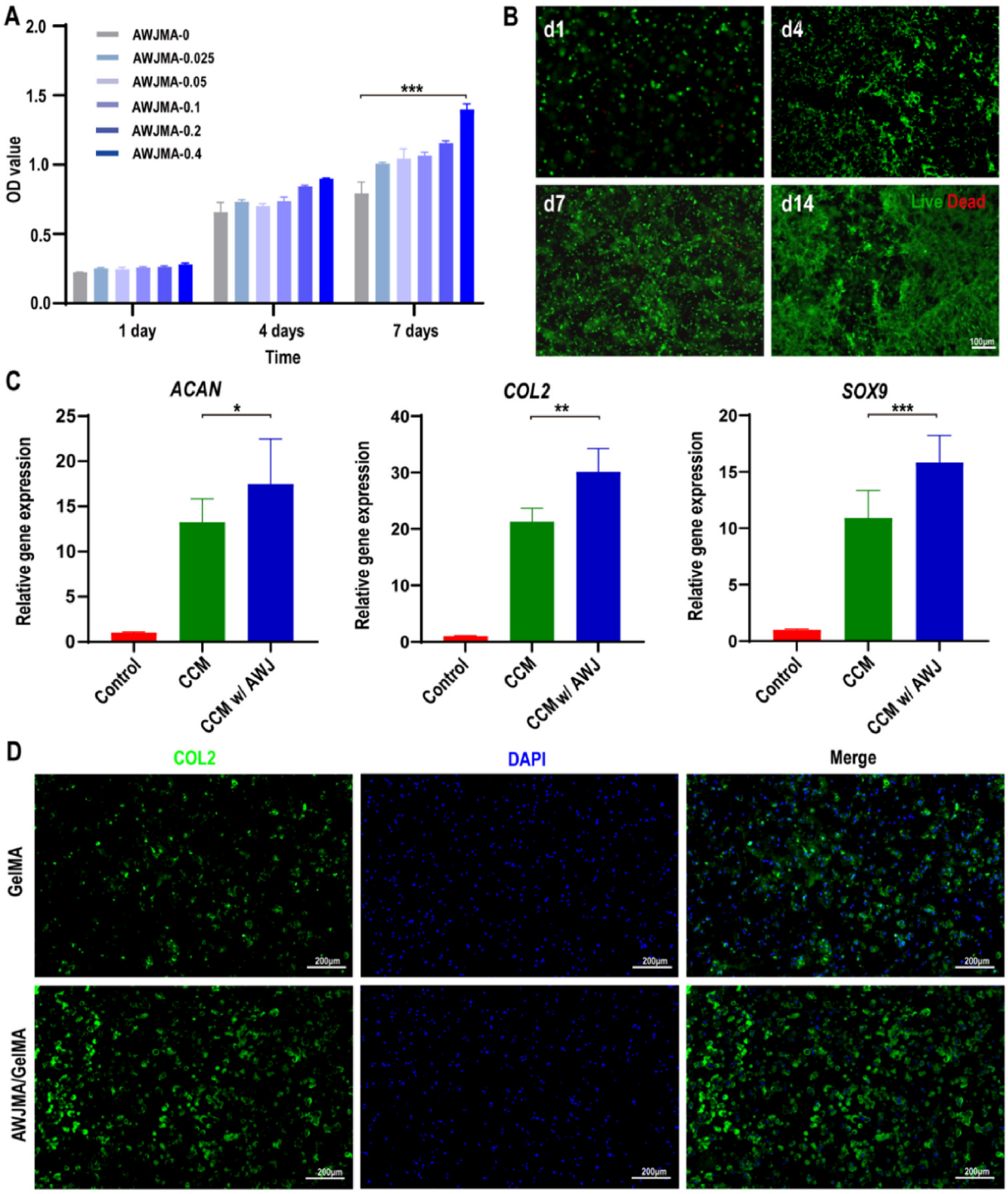


**Fig. 5. Biological properties of AWJMA/GelMA hydrogels.** A) CCK-8 tests of **AWJMA** polymers at different concentrations show satisfactory cytocompatibility. B) Live/dead fluorescence staining shows the viability of encapsulated BMSCs on days 1, 4, 7, and 14, with live cells in green and dead cells in red. C) Expression of cartilage-specific genes (*ACAN*, *COL2*, and *SOX9*) induced by 0.4 wt% **AWJ** polymer. D) Collagen II immunofluorescence staining of BMSCs-loaded **GelMA** and **AWJMA/GelMA** hydrogels after 28 days of culturing (green: COL2; blue: DAPI). $^{*}p < 0.05$, $^{**}p < 0.01$, $^{***}p < 0.001$.

swelling ratios and degradation rates for 3D bioprinting. Furthermore, optimization of 3D bioprinting parameters enabled the printing of BMSCs-loaded cartilage-mimicking substitutes with superior advantages for BMSC survival, proliferation, spreading, and chondrogenic differentiation. Finally, a model of full-thickness articular cartilage defect in the rabbit knee joint was satisfactorily repaired using the BMSCs-loaded 3D-bioprinted cartilage-mimicking substitute. Thus, the current study provides novel cartilage-mimicking hydrogel materials and 3D-bioprinted substitutes as an alternative treatment for articular cartilage repair.

How to prepare photo-crosslinkable Wharton's jelly as bioinks for 3D bioprinting is the first challenge that we faced. First, we selected Wharton's jelly to prepare photo-crosslinkable hydrogels for the following two reasons: 1) In contrast to animal-derived cartilage or derm acellular

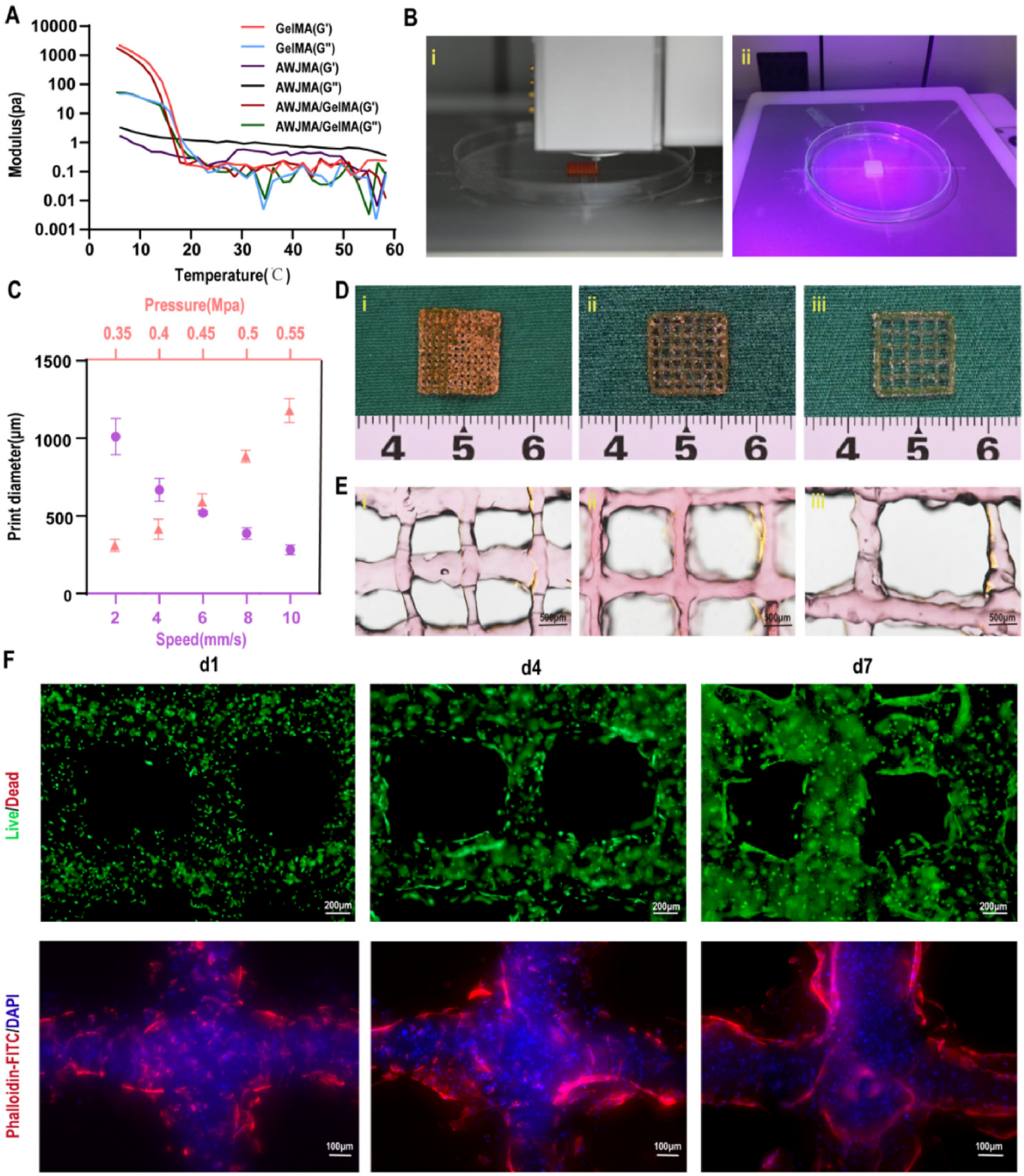


**Fig. 6. 3D bioprinting of BMSCs-loaded AWJMA/GelMA hydrogels.** A) Temperature-sweep rheological analyses indicate that the printability of **AWJMA/GelMA** hydrogels is based on the temperature-sensitive property. B) Photographs of 3D bioprinting by light-assisted extrusion molding. C) Optimization of the main printing parameters of **AWJMA/GelMA** hydrogels, namely printing speed and pressure. D, E) The gross view (D) and microscope images (E) of 3D-bioprinted lattice constructs with different gaps, namely 1.0 mm (i), 1.5 mm (ii), and 2.0 mm (iii). F) Live/dead and phalloidin staining of 3D-bioprinted lattice constructs with BMSC encapsulation after 1, 4, and 7 days of culturing *in vitro*.

matrices, human-derived Wharton's jelly is biocompatible and hypoimmunogenic with an abundant source [37]. 2) Wharton's jelly contains cartilage-like components and several chondrogenic growth factors that benefit cartilage regeneration. However, it is difficult to construct complex architectures from widely used powder-like Wharton's jelly by means of the prevailing technique of 3D bioprinting. Therefore, it is necessary to prepare Wharton's jelly into soluble components as bioinks. By referring to our groups' previously established photo-crosslinking strategies for constructing acellular matrix-based hydrogels [38], **AWJMA** was successfully prepared through a multi-step procedure of decellularization, enzymatic digestion, MA modification, and lyophilization, which was confirmed with $^{1}$H NMR and FTIR spectra. The results of proteomics analysis further verified that acellular Wharton's jelly reserved most of the ECM components found in the cartilage matrix and contained chondrogenic active substances conductive to cartilage regeneration.

Whether photo-crosslinkable Wharton's jelly-based bioinks could realize 3D-bioprinting of cartilage-mimicking substitutes is the next

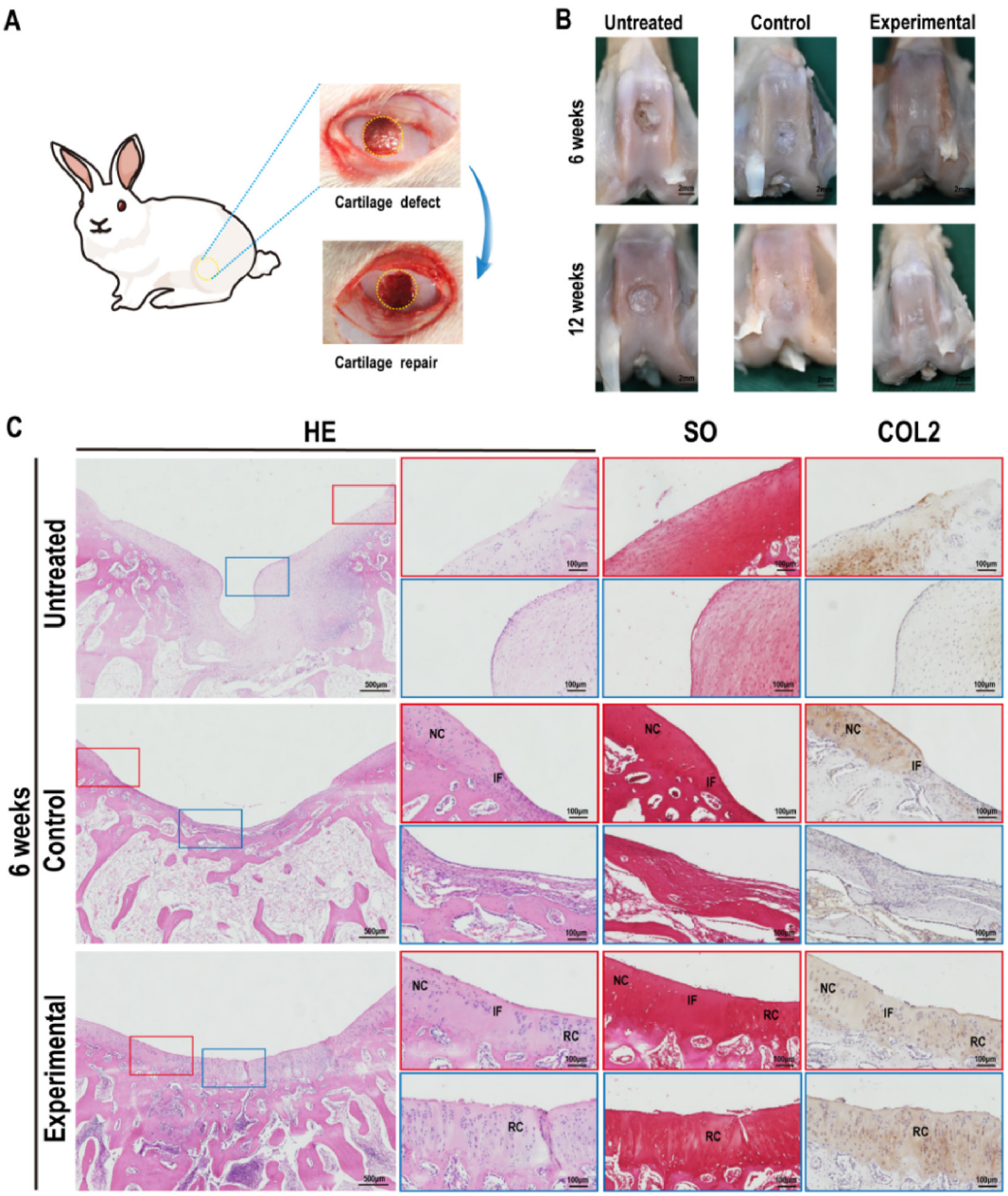


**Fig. 7. Gross morphology and histological examinations of samples at 6 weeks.** A) Full-thickness cartilage defects on rabbit knee joints were created and repaired by the 3D-bioprinted cartilage-mimicking substitute. B) Gross views of the articular cartilage at 6 and 12 weeks post-surgery. C) Representative histological images of H&E staining, Safranin-O staining, and type II collagen immunofluorescence staining of the cartilage defect areas of Untreated, Control, and Experimental groups at 6 weeks post-surgery. RC: repaired cartilage; IF: interface; NC: native cartilage.

important issue. Although **AWJMA** hydrogels possessed ideal biocompatibility and chondrogenic activity, it exhibited low viscosity without temperature-sensitive properties for supporting extrusion and resisting collapse. To address the above problem, printable **GelMA** was introduced into **AWJMA** to form hybrid **GelMA/AWJMA** hydrogels, which exhibited temperature-sensitive sol-to-gel transitions suitable for extrusion-based 3D bioprinting, as well as rapid photo-crosslinking to sustain specific 3D shapes. Additionally, the combination of **GelMA** and **AWJMA** provided a hydrogel that exhibited not only suitable rheological and mechanical properties but also reasonable swelling ratios and degradation rates. The current results demonstrated that 3D-bioprinted lattice structures with high fidelity and clear resolution were successfully achieved by optimizing relevant parameters, such as applied pressure, printing speed, and interfilament gap. The *in vitro* experiments further confirmed that the BMSCs-loaded cartilage-mimicking substitute exhibited superior advantages for BMSC survival, proliferation, and spreading, which depended on the interconnected channels within the 3D-bioprinted architecture. More importantly, Wharton's jelly-based hydrogels contained IGF and TGFβ active substances, which facilitated the chondrogenic differentiation of BMSCs to some extent.

Finally, whether the 3D-bioprinted cartilage-mimicking substitute could repair full-thickness articular cartilage defects was a very important preclinical consideration. In this study, BMSCs were selected as seed cells for the construction of 3D-bioprinted cartilage-mimicking substitute because autogenous BMSCs are easily obtained by minimally invasive approach, as well as a definite chondrogenic differentiation potential under the *in situ* cartilage-specific microenvironment. The current results demonstrated that cartilage defects in both BMSCs-loaded and BMSCs-free groups were satisfactory repaired with cartilage-specific matrix deposition and clear epiphyseal line-like structures at 12 weeks, whereas

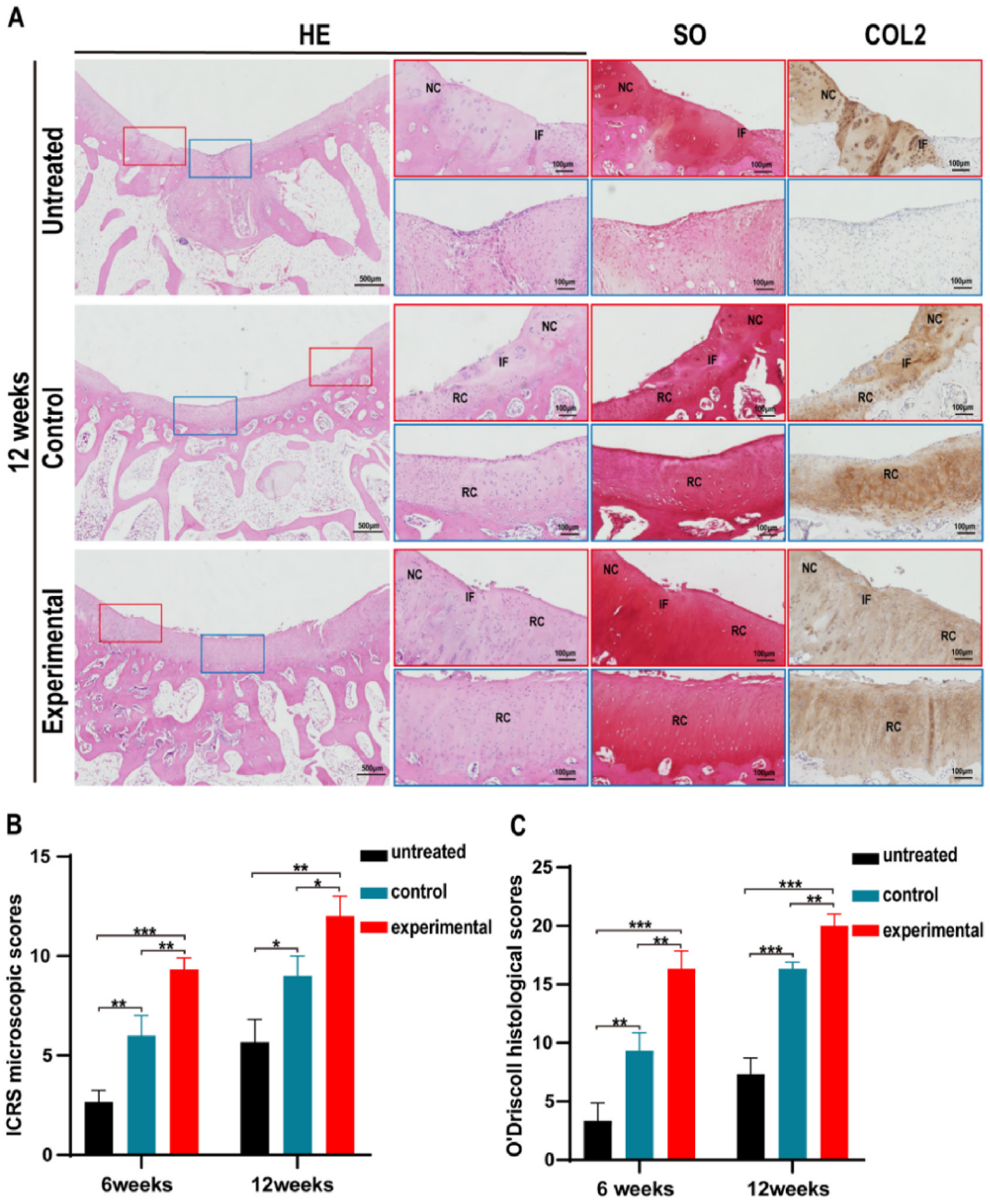


**Fig. 8. Histological examinations of samples at 12 weeks post-surgery and histological scores at 6 and 12 weeks post-surgery.** A) Representative histological images of H&E staining, Safranin-O staining, and type II collagen immunofluorescence staining of the cartilage defect areas of Untreated, Control, and Experimental groups at 12 weeks post-surgery. RC: repaired cartilage; IF: interface; NC: native cartilage. B) International Cartilage Repair Society (ICRS) scores of samples at 6 and 12 weeks post-surgery. C) Modified O'Driscoll histology scoring system (MODS) scores of samples at 6 and 12 weeks post-surgery. *$p < 0.05$, **$p < 0.01$, ***$p < 0.001$.

defects in the untreated group were repaired with disorganized fibrous-like tissue. Notably, BMSCs-loaded groups achieved defect repair with mature hyaline cartilage at 6 weeks, indicating that the cartilage defect repair rate was faster, and the regenerated cartilage thickness and quality were better than those of the BMSCs-free group. This is attributed to the following reasons: 1) 3D-bioprinted lattice structures have interconnected channels that facilitate the enrichment of local autologous stem cells from the injured subchondral bone, as well as nutrient transport in joints. 2) The addition of extra BMSCs provides sufficient seed cells for cartilage defect repair. 3) Stem cell differentiation and cartilage-specific repair are mediated by Wharton's jelly-based scaffolds and the *in situ* microenvironment.

## 5. Conclusion

In summary, we developed novel 3D-bioprinted cartilage-mimicking substitutes for full-thickness articular cartilage defect repair. Human-derived Wharton's jelly is biocompatible and hypoimmunogenic with an abundant source, which has a broad prospect for clinical applications and cartilage tissue engineering. Furthermore, the hybrid design of photo-crosslinkable **GelMA** and **AWJMA** components facilitates the 3D printing of cartilage-mimicking substitutes with suitable physicochemical properties and ideal biological activities, which enables full-thickness articular cartilage defect repair. In future, this strategy together with other advanced techniques (*e.g.*, microfracture and

arthroscopy) will enable 3D bioprinting of individually customized elaborate cartilage-mimicking substitutes with larger sizes and more complex morphologies for articular cartilage defect repair. Although the current work represents a proof-of-concept study using the rabbit models, after a preclinical evaluation in a big animal model with a long-term follow up, we can envision that 3D bioprinting is a promising strategy for articular cartilage defect repair.

## Credit author statement

G. H., Y. H., G. Z., and W. R. designed the experiments. G. H., Q. P., M. Y., and Y. H. performed the experiments. G. H., Z. L., L. F., Y. N, W. Z., L. W., X. W., and Y. H. analyzed the data. G. H., Y. H., G. Z., and W. R. wrote the manuscript.

## Declaration of competing interest

The authors declare that they have no known competing financial interests or personal relationships that could have appeared to influence the work reported in this paper.

## Data availability

The data that has been used is confidential.

## Acknowledgements

This research was financially supported by the Key Research and Development Program of Henan province (No. 221111310100), Major Science and Technology Projects of Xinxiang City (No. 21ZD006), the Open Research Fund of Tissue Engineering and Regenerative Clinical Medical Center of Xinxiang Medical University (No.2022KFKTZD02; No.2022YFYKFKT01), the Key Scientific Research Projects of Universities in Henan Province (No.23B416002), the National Key Research and Development Program of China (2022YFA1207500, 2018YFC1105800), the National Natural Science Foundation of China (81871502 and 81671837), the Shanghai Collaborative Innovation Program on Regenerative Medicine and Stem Cell Research (2019CXJQ01), the Clinical Research Plan of SHDC (No.SHDC2020CR2045B), and Shanghai Municipal Key Clinical Specialty (shslczdzk06601).

## References

[1] F.T. Moutos, F. Guilak, Composite scaffolds for cartilage tissue engineering, Biorheology 45 (2008) 501–512. http://10.3233/BIR-2008-0491.
[2] A. Trengove, C. Di Bella, A.J. O'Connor, The challenge of cartilage integration: understanding a major barrier to chondral repair, Tissue Eng. B Rev. 28 (2022) 114–128. http://10.1089/ten.teb.2020.0244.
[3] K. Abe, A. Yamashita, M. Morioka, N. Horike, Y. Takei, S. Koyamatsu, K. Okita, S. Matsuda, N. Tsumaki, Engraftment of allogeneic iPS cell-derived cartilage organoid in a primate model of articular cartilage defect, Nat. Commun. 14 (2023). http://10.1038/s41467-023-36408-0.
[4] A. Bedi, B.T. Feeley, R.J. Williams, Management of articular cartilage defects of the knee, The Journal of Bone and Joint Surgery-American 92 (2010) 994–1009. http://10.2106/JBJS.I.00895.
[5] Y. Liu, K.M. Shah, J. Luo, Strategies for articular cartilage repair and regeneration, Front. Bioeng. Biotechnol. 9 (2021). http://10.3389/fbioe.2021.770655.
[6] K. Ye, R. Felimban, S.E. Moulton, G.G. Wallace, C.D. Bella, K. Traianedes, P.F. Choong, D.E. Myers, Bioengineering of articular cartilage: past, present and future, Regen. Med. 8 (2013) 333–349. http://10.2217/rme.13.28.
[7] C.D. O'Connell, S. Duchi, C. Onofrillo, L.M. Caballero Aguilar, A. Trengove, S.E. Doyle, W.J. Zywicki, E. Pirogova, C. Di Bella, Within or without you? A perspective comparing in situ and ex situ tissue engineering strategies for articular cartilage repair, Adv. Healthc. Mater. 11 (2022), 2201305. http://10.1002/adhm.202201305.
[8] H. Kwon, W.E. Brown, C.A. Lee, D. Wang, N. Paschos, J.C. Hu, K.A. Athanasiou, Surgical and tissue engineering strategies for articular cartilage and meniscus repair, Nat. Rev. Rheumatol. 15 (2019) 550–570. http://10.1038/s41584-019-0255-1.
[9] X. Nie, Y.J. Chuah, W. Zhu, P. He, Y. Peck, D. Wang, Decellularized tissue engineered hyaline cartilage graft for articular cartilage repair, Biomaterials 235 (2020), 119821. http://10.1016/j.biomaterials.2020.119821.
[10] W. Wei, Y. Ma, X. Zhang, W. Zhou, H. Wu, J. Zhang, J. Lin, C. Tang, Y. Liao, C. Li, X. Wang, X. Yao, Y.W. Koh, W. Huang, H. Ouyang, Biomimetic joint paint for efficient cartilage repair by simultaneously regulating cartilage degeneration and regeneration in pigs, ACS Appl. Mater. Interfaces 13 (2021) 54801–54816. http://10.1021/acsami.1c17629.
[11] L. Li, J.M. Scheiger, P.A. Levkin, Design and applications of photoresponsive hydrogels, Adv. Mater. 31 (2019), 1807333. http://10.1002/adma.201807333.
[12] M. Liu, X. Zeng, C. Ma, H. Yi, Z. Ali, X. Mou, S. Li, Y. Deng, N. He, Injectable hydrogels for cartilage and bone tissue engineering, Bone Research 5 (2017). http://10.1038/boneres.2017.14.
[13] Q. Mei, J. Rao, H.P. Bei, Y. Liu, X. Zhao, 3D bioprinting photo-crosslinkable hydrogels for bone and cartilage repair, Int J Bioprint 7 (2021) 367. http://10.18063/ijb.v7i3.367.
[14] M. Li, D. Sun, J. Zhang, Y. Wang, Q. Wei, Y. Wang, Application and development of 3D bioprinting in cartilage tissue engineering, Biomater. Sci.-UK 10 (2022) 5430–5458. http://10.1039/D2BM00709F.
[15] A. Zelinka, A.J. Roelofs, R.A. Kandel, C. De Bari, Cellular therapy and tissue engineering for cartilage repair, Osteoarthritis Cartilage 30 (2022) 1547–1560. http://10.1016/j.joca.2022.07.012.
[16] M. Shie, W. Chang, L. Wei, Y. Huang, C. Chen, C. Shih, Y. Chen, Y. Shen, 3D printing of cytocompatible water-based light-cured polyurethane with hyaluronic acid for cartilage tissue engineering applications, Materials 10 (2017) 136. http://10.3390/ma10020136.
[17] Z. Lin, M. Wu, H. He, Q. Liang, C. Hu, Z. Zeng, D. Cheng, G. Wang, D. Chen, H. Pan, C. Ruan, 3D printing of mechanically stable calcium-free alginate-based scaffolds with tunable surface charge to enable cell adhesion and facile biofunctionalization, Adv. Funct. Mater. 29 (2019), 1808439, https://doi.org/10.1002/adfm.201808439.
[18] Y. Liu, L. Peng, L. Li, C. Huang, K. Shi, X. Meng, P. Wang, M. Wu, L. Li, H. Cao, K. Wu, Q. Zeng, H. Pan, W.W. Lu, L. Qin, C. Ruan, X. Wang, 3D-bioprinted BMSC-laden biomimetic multiphasic scaffolds for efficient repair of osteochondral defects in an osteoarthritic rat model, Biomaterials 279 (2021), 121216, https://doi.org/10.1016/j.biomaterials.2021.121216.
[19] N. Ding, E. Li, X. Ouyang, J. Guo, B. Wei, The therapeutic potential of bone marrow mesenchymal stem cells for articular cartilage regeneration in osteoarthritis, Curr. Stem Cell Res. Ther. 16 (2021) 840–847. http://10.2174/1574888X16666210127130044.
[20] T.P. Liu, P. Ha, C.Y. Xiao, S.Y. Kim, A.R. Jensen, J. Easley, Q. Yao, X. Zhang, Updates on mesenchymal stem cell therapies for articular cartilage regeneration in large animal models, Front. Cell Dev. Biol. 10 (2022). http://10.3389/fcell.2022.982199.
[21] O. Messaoudi, C. Henrionnet, K. Bourge, D. Loeuille, P. Gillet, A. Pinzano, Stem cells and extrusion 3D printing for hyaline cartilage engineering, Cells 10 (2021) 2. http://10.3390/cells10010002.
[22] M. Xie, K. Yu, Y. Sun, L. Shao, J. Nie, Q. Gao, J. Qiu, J. Fu, Z. Chen, Y. He, Protocols of 3D bioprinting of gelatin methacryloyl hydrogel based bioinks, JoVE 154 (2019) 1–6, https://doi.org/10.3791/60545.
[23] G. Ying, N. Jiang, C. Yu, Y.S. Zhang, Three-dimensional bioprinting of gelatin methacryloyl (GelMA), Bio-Design and Manufacturing 1 (2018) 215–224. http://10.1007/s42242-018-0028-8.
[24] A. Erdem, M.A. Darabi, R. Nasiri, S. Sangabathuni, Y.N. Ertas, H. Alem, V. Hosseini, A. Shamloo, A.S. Nasr, S. Ahadian, M.R. Dokmeci, A. Khademhosseini, N. Ashammakhi, 3D bioprinting of oxygenated cell-laden gelatin methacryloyl constructs, Adv. Healthc. Mater. 9 (2020), 1901794. http://10.1002/adhm.201901794.
[25] L. Xu, Z. Zhang, A.M. Jorgensen, Y. Yang, Q. Jin, G. Zhang, G. Cao, Y. Fu, W. Zhao, J. Ju, R. Hou, Bioprinting a skin patch with dual-crosslinked gelatin (GelMA) and silk fibroin (SilMA): an approach to accelerating cutaneous wound healing, Materials Today Bio 18 (2023), 100550. http://10.1016/j.mtbio.2023.100550.
[26] K. Ma, T. Zhao, L. Yang, P. Wang, J. Jin, H. Teng, D. Xia, L. Zhu, L. Li, Q. Jiang, X. Wang, Application of robotic-assisted in situ 3D printing in cartilage regeneration with HAMA hydrogel: an in vivo study, J. Adv. Res. 23 (2020) 123–132. http://10.1016/j.jare.2020.01.010.
[27] W. Kim, H. Lee, J. Lee, A. Atala, J.J. Yoo, S.J. Lee, G.H. Kim, Efficient myotube formation in 3D bioprinted tissue construct by biochemical and topographical cues, Biomaterials 230 (2020), 119632. http://10.1016/j.biomaterials.2019.119632.
[28] Y. Hua, Y. Huo, B. Bai, J. Hao, G. Hu, Z. Ci, X. Wu, M. Yu, X. Wang, H. Chen, W. Ren, Y. Zhang, X. Wang, G. Zhou, Fabrication of biphasic cartilage-bone integrated scaffolds based on tissue-specific photo-crosslinkable acellular matrix hydrogels, Materials Today Bio 17 (2022), 100489. http://10.1016/j.mtbio.2022.100489.
[29] K. Behan, A. Dufour, O. Garcia, D. Kelly, Methacrylated cartilage ECM-based hydrogels as injectables and bioinks for cartilage tissue engineering, Biomolecules 12 (2022) 216. http://10.3390/biom12020216.
[30] A. Gupta, N. Maffulli, H.C. Rodriguez, E.W. Carson, R.A. Bascharon, K. Delfino, H.J. Levy, S.F. El-Amin, Safety and efficacy of umbilical cord-derived Wharton's jelly compared to hyaluronic acid and saline for knee osteoarthritis: study protocol for a randomized, controlled, single-blind, multi-center trial, J. Orthop. Surg. Res. 16 (2021). http://10.1186/s13018-021-02475-6.
[31] A. Gupta, N. Maffulli, H.C. Rodriguez, C.E. Lee, H.J. Levy, S.F. El-Amin, Umbilical cord-derived Wharton's jelly for treatment of knee osteoarthritis: study protocol for a non-randomized, open-label, multi-center trial, J. Orthop. Surg. Res. 16 (2021). http://10.1186/s13018-021-02300-0.
[32] A. Gupta, S.F. El-Amin, H.J. Levy, R. Sze-Tu, S.E. Ibim, N. Maffulli, Umbilical cord-derived Wharton's jelly for regenerative medicine applications, J. Orthop. Surg. Res. 15 (2020). http://10.1186/s13018-020-1553-7.

[33] Z. Li, Y. Bi, Q. Wu, C. Chen, L. Zhou, J. Qi, D. Xie, H. Song, Y. Han, P. Qu, K. Zhang, Y. Wu, Q. Yin, A composite scaffold of Wharton's jelly and chondroitin sulphate loaded with human umbilical cord mesenchymal stem cells repairs articular cartilage defects in rat knee, J. Mater. Sci. Mater. Med. 32 (2021). http://10.1007/s10856-021-06506-w.

[34] P. Zhao, S. Liu, Y. Bai, S. Lu, J. Peng, L. Zhang, J. Huang, B. Zhao, W. Xu, Q. Guo, hWJECM-derived oriented scaffolds with autologous chondrocytes for rabbit cartilage defect repairing, Tissue Eng. 24 (2018) 905–914. http://10.1089/ten.tea.2017.0223.

[35] Y. Xu, L. Duan, Y. Li, Y. She, J. Zhu, G. Zhou, G. Jiang, Y. Yang, Nanofibrillar decellularized wharton's jelly matrix for segmental tracheal repair, Adv. Funct. Mater. 30 (2020), 1910067. http://10.1002/adfm.201910067.

[36] A.I. Van Den Bulcke, B. Bogdanov, N. De Rooze, E.H. Schacht, M. Cornelissen, H. Berghmans, Structural and rheological properties of methacrylamide modified gelatin hydrogels, Biomacromolecules 1 (2000) 31–38. http://10.1021/bm990017d.

[37] M. Dubus, L. Scomazzon, J. Chevrier, C. Ledouble, A. Baldit, J. Braux, F. Gindraux, C. Boulagnon, S. Audonnet, M. Colin, H. Rammal, C. Mauprivez, H. Kerdjoudj, Antibacterial and immunomodulatory properties of acellular Wharton's jelly matrix, Biomedicines 10 (2022) 227. http://10.3390/biomedicines10020227.

[38] Y. Huo, Y. Xu, X. Wu, E. Gao, A. Zhan, Y. Chen, Y. Zhang, Y. Hua, W. Swieszkowski, Y.S. Zhang, G. Zhou, Functional Trachea Reconstruction Using 3D-Bioprinted Native-Like Tissue Architecture Based on Designable Tissue-Specific Bioinks, Advanced Science, 2022, 2202181. http://10.1002/advs.202202181.